A Comparison of Electrostatically Charged Metal Materials for Collecting Tire Wear Particles

Brandon Situ[a]
[a]Upper Canada College, M4V 1W6, Toronto, ON, Canada
bdnsitu@gmail.com

Abstract

This study compares the effect of applying 5 kV for four electrostatically charged metal materials (aluminum, brass, copper, and stainless steel) on capturing tire wear particles (TWPs) behind the wheel. A smooth-tread bicycle tire was spun against sandpaper while two metal plates collected the TWPs. Particles were measured in ImageJ by the percentage of the plate surface covered and the number of particles. Across the materials, charging raised surface coverage 23.2-fold and particle count 15.8-fold (both $p < 0.001$). The size of the gain depended on the material for both metrics (interaction $p = 0.007$ for coverage; $p < 0.001$ for count). All four materials improved significantly on surface coverage; brass, copper, and stainless steel improved on particle count. Copper gained the most at 114 times the surface coverage and 53.6 times the count. For aluminum, its surface coverage increased 5.5 times ($p = 0.001$) but its particle count only increased 2.0 times and did not reach significance. Once charged, copper and brass yielded about twenty times more TWP material than aluminum or stainless steel. In every charged trial for all materials, it was found that particles were only collected on the negatively charged plate, suggesting that the generated TWPs were positively charged. The results emphasize the importance of plate material in electrostatic TWP collector designs.

Keywords: tire wear particles; electrostatic capture; collector plate material; triboelectric charging; non-exhaust emissions

1. Introduction

Particles from brakes, tires, and road surfaces have become a growing environmental concern, with up to 90% of traffic-related particles being attributed to tire wear particles (TWPs) by mass in some countries [1]. Giechaskiel et al. [2] used about 300 recent measurements and found an average abrasion rate of 110 mg per kilometer per car and that tire wear accounts for between a third and a half of all microplastics released unintentionally into the environment. The European Union has set tire abrasion limits through Euro 7, the first regulation to mitigate this issue. Prototypes of near-wheel TWP capture devices exist, but the technology is still in its developing stages.

The harmful effects of TWPs are attributed to their composition. Tire and road wear particles (TRWPs) contain zinc, polycyclic aromatic hydrocarbons, and a range of leftover additives from vulcanization [3]. Specifically, 6PPD is an antioxidant additive whose breakdown product 6PPD-quinone was found to explain decades of coho salmon deaths in urban creeks, killing at concentrations below one microgram per liter [4]. Studies on human airway organoids and lung macrophages report effects such as oxidative stress and inflammation, with the finest particles provoking the strongest responses [5,6].

Currently, two types of capture devices exist. Aerodynamic designs funnel the air behind the tire into a duct. A wheel-cover channel of this kind captured more than 40% of TWPs in simulations and on the road at highway speeds [7]. Electrostatic designs use high-voltage metal plates to capture charged TWPs. The Tyre Collective

has developed devices that mount these plates behind a wheel, which captured 60% of airborne TWPs during testing [8]. A collector that used suction and an electrostatic precipitator was able to remove over 95% of brake wear particles in dynamometer tests and reduce emissions by 75% on a vehicle [9]. A later version reduced the on-road PM10 emission factor by 59% [10].

Minimal studies have compared collector plate materials of electrostatically charged plates. The Tyre Collective's patent lists copper, brass, steel, aluminum, metal alloys, and conductive polymers [8], though there is limited testing to determine which material is the most effective. The literature on precipitators does not provide a definitive optimal electrode material. For example, Lee et al. tested a two-stage precipitator on oil mist and showed that electrode material made minimal difference, with plastic and carbon matching the performance of stainless steel [11]. Syu et al. compared stainless steel, conductive glass, and regular glass and found large differences, where particle penetration was below 6% for the two conducting surfaces but above 40% for the insulating one [12].

2. Background

Electrostatic TWP capture relies on triboelectric charging that occurs when two surfaces contact and separate. During abrasion, charge is transferred across the interface, generating a charge in the particle. A charged particle entering the gap between two high-voltage parallel plates experiences a force proportional to its charge and the electric field strength. For two parallel plates, increasing the applied voltage or decreasing the gap increases its field strength. Molecular dynamics simulations of the contact between natural rubber and copper show that charge transfer reduces the system's electrostatic potential energy [13]. The amount of charge transferred depends on the contact pressure and roughness of the counter-surface [14]. The collector designed by The Tyre Collective uses plates of alternating polarity to capture TWPs of both charges [8].

An industrial electrostatic precipitator is described by the Deutsch equation [15], where collection efficiency increases with plate area and drift velocity of charged particles and decreases as air velocity increases. This equation assumes a corona stage that imposes a known charge on each particle before they reach the collecting plates. The present study has no corona stage as the particles are charged before arriving and the plates are used to attract them. Therefore, the particle retention is more important than its drift velocity. Bailey [16] described that retention is a combination of electrostatic image forces and van der Waals attraction.

A material property that may contribute to differences in capture performance is the surface oxide layer that forms naturally on each metal. It is insulating on aluminum and more conductive on stainless steel, brass, and copper. This is discussed in Section 5.1.

3. Methodology

3.1 Experimental design

Figure 1 presents a schematic diagram of the experiment. TWPs were produced by spinning a smooth-tread bicycle tire (Specialized) against P120 sandpaper with a synchronous motor (CHANCS) at 100 revolutions per minute. A bicycle tire was employed because it allows for a compact rig with controllable speed and contact force; the implications are discussed in Section 5.3.

The experiment had two independent variables, material and voltage. The four materials (aluminum, brass, copper, and stainless steel) were chosen as they are primarily used in electrostatic capture designs [8]. Each material was tested uncharged (0 kV) and charged (5 kV, measured with a Fluke 80K-40). Each trial was 120 s and conditions were repeated three times. Rotation speed, run time, sandpaper grit, tire, and plate size were held constant.

Plates were 150 × 150 × 0.5 mm and were used in pairs of the same material, separated by 3 cm. Each pair was positioned parallel to the trajectory of the particles leaving the tire. Voltage was supplied by a signal generator (UCTRONICS) and a DC high-voltage generator (Jectse). A potential difference was applied across the plates by connecting each to the opposite terminals of the power supply. The plates were discharged and cleaned before every trial.

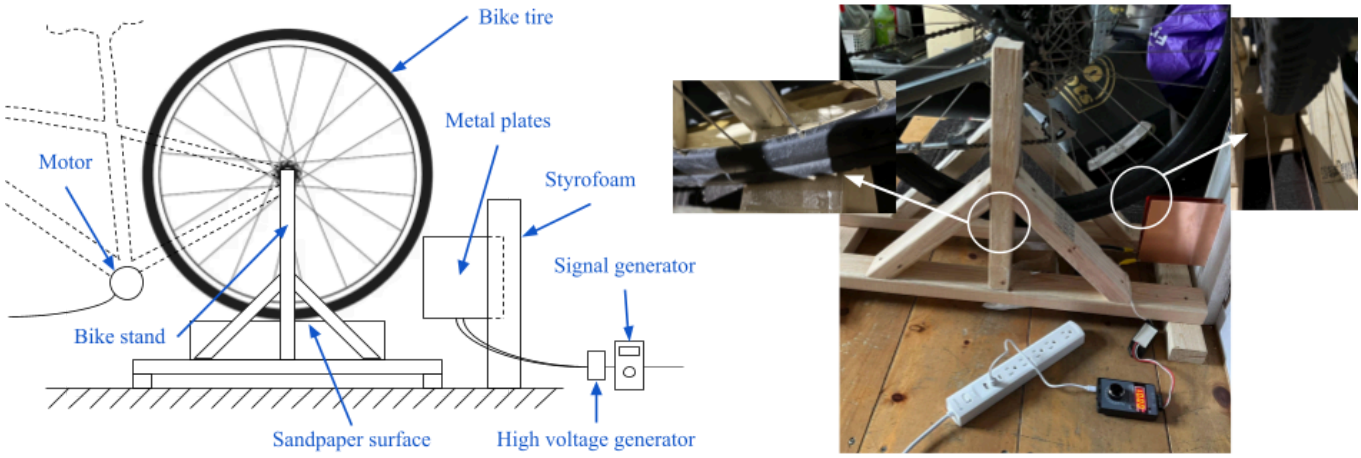

(a) The schematic diagram of the apparatus

(b) The physical equipment

Figure 1. The experimental apparatus.

3.2 Photography and particle measurement

For every trial during the experiment, particles were only visible on the negatively charged plate of each pair. In the charged trials, all measurements are reported from the negatively charged plate. In the uncharged trials, measurements are reported for the plate in the same position. This result is described in Section 4.1.

Each plate was photographed at 3840 × 2160 pixels resolution with a 45° angle between the camera and plate to reduce glare and allow individual particles to be distinguished from the metal. The images were processed in Adobe Photoshop to correct perspective using the Guided Upright tool. Corrected images were analyzed in ImageJ [17] where each was converted to 8-bit grayscale and automatically thresholded using Otsu's method to isolate the particles. The Analyze Particles command was run with a size limit of 1 cm2 and the image scale was defined using the plate dimensions. Non-particle features such as reflections were manually removed and segmentation was verified using the original photograph.

3.3 Metrics used

The first metric used is the percentage of collector plate area occupied by the particles. Because this metric is dimensionless, images can be compared without normalization. At constant particle thickness, it is proportional to the mass of material held. It also does not increase if the same amount of material breaks into separate pieces. The second metric is the number of particles counted. This metric is less influenced by large particles that may affect surface coverage. Agreement between the two metrics increases confidence in trends, while discrepancies are noted.

3.4 Statistical analysis

The primary analysis is a two-way analysis of variance (ANOVA) with material, voltage, and their interaction as factors. ANOVA assumes additivity and homogenous variance, though it was found that charging multiplies capture by a factor instead of adding an amount. Conditions with higher mean capture values were more variable (mean and standard deviation correlation: $r = 0.87$) and residuals were not normally distributed (Shapiro–Wilk $p = 0.00005$ for coverage; $p = 0.0003$ for count). Thus, measurements were transformed using base-10 logarithms. Averages are reported as a geometric mean because the data differ proportionally. Shapiro–Wilk and Levene's tests were applied to the transformed data.

The effect of charging each material is expressed as an improvement factor, the ratio of the charged to uncharged geometric means. The 95% confidence intervals (CIs) were calculated using Welch's t test on the log-transformed values. The materials were compared in the charged state using Tukey's honestly significant difference (HSD) test. Analysis code was developed with the assistance of Claude (Anthropic) and reviewed by the author prior to use. Calculations were performed in Python 3.9.6 (NumPy 2.0.2; SciPy 1.13.1; pandas 2.3.3; statsmodels 0.14.6).

4. Results

4.1 Single-plate collection

Figure 2 (a) shows a pair of copper plates after a trial, with captured particles visible on solely the negatively charged plate. This result should be regarded as qualitative as the positively charged plates were not imaged and quantified. The implications for the polarity are discussed in Section 5.2.

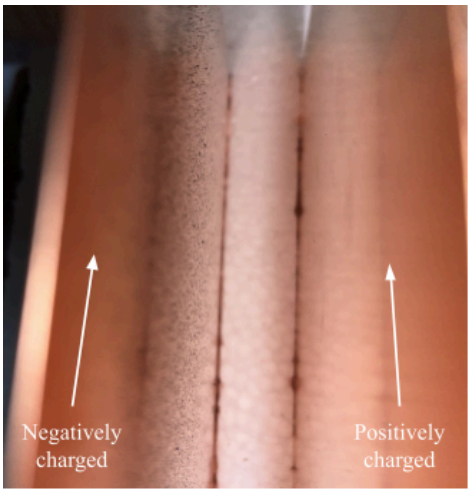

(a) Collector plates for copper trial 4

(b) Negative copper plate in trial 4

Figure 2. TWPs adhering to the negatively charged collector plates when charged.

4.2 Summary of the data

Figure 3 shows the plate outline masks for each condition. Table 1 and Figure 4 present geometric means and ranges of each material for both uncharged and charged conditions. After charging, both surface coverage and particle count increased for brass, copper, and stainless steel. They increased for aluminum as well but by smaller amounts. Copper yielded the largest surface coverage when charged (1.250%) and brass produced the highest particle count when charged (4571).

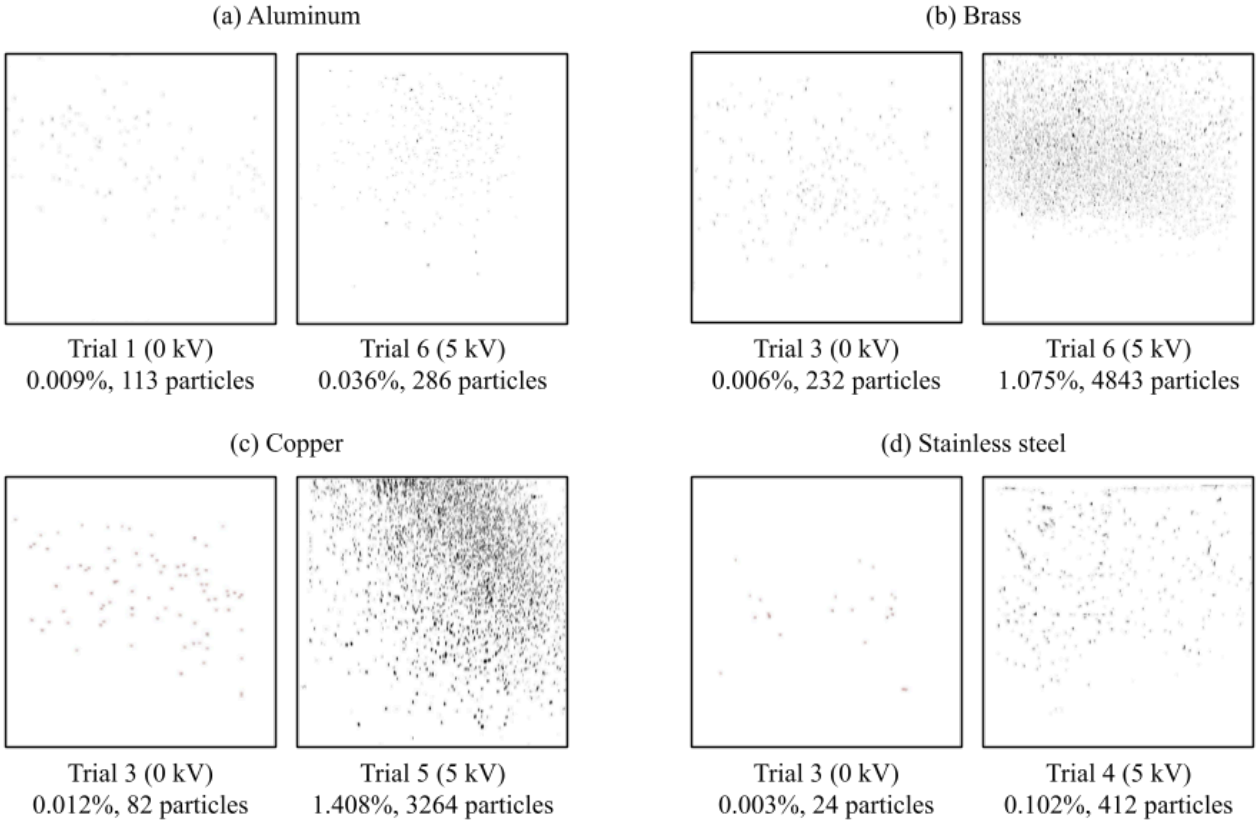

Figure 3. Thresholded images for representative trials for each condition (n = 3) with surface coverage (%) and particle count.

Material	Voltage	Surface coverage (%), geometric mean (range)	Particle count, geometric mean (range)	Area covered (mm^2)	Average particle diameter (µm)
Aluminum	0 kV	0.0069 (0.006–0.009)	94 (78–113)	1.5	340
Aluminum	5 kV	0.0377 (0.033–0.045)	184 (102–286)	8.5	510
Brass	0 kV	0.049 (0.013–0.130)	172 (96–232)	11.0	650
Brass	5 kV	0.892 (0.452–1.461)	4571 (3971–4967)	200.7	370
Copper	0 kV	0.011 (0.005–0.022)	51 (18–90)	2.5	540
Copper	5 kV	1.250 (0.959–1.448)	2736 (2030–3264)	281.3	840
Stainless steel	0 kV	0.003 (0.003–0.004)	23 (21–24)	0.7	400
Stainless steel	5 kV	0.085 (0.033–0.181)	505 (412–587)	19.1	450

Table 1. Summary of evaluation metrics by plate material and voltage (n = 3 per condition). Surface coverage is the percentage of the total plate area covered by the particles.

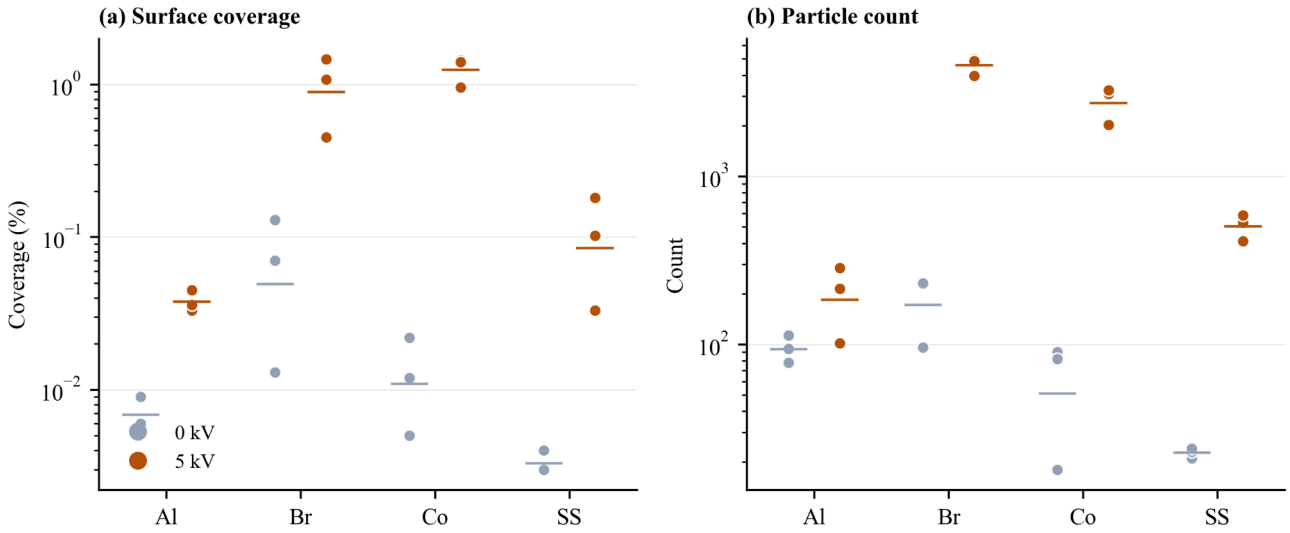

Figure 4. Surface coverage (a) and particle count (b) by plate material and voltage. Points are individual trials, horizontal bars are geometric means. Vertical axes are logarithmic.

4.3 Effect of charging

Charging the plates increased capture substantially for all four materials on surface coverage and three out of four on particle count. On average, across all materials, charging increased surface coverage 23.2-fold and particle count 15.8-fold.

Table 2 reports the two-way ANOVA for both metrics on the log-transformed data. Voltage explained more variance than material for both metrics. The effect was greater for particle count ($F(1,16) = 242.55$, $p < 0.001$, $\eta_p^2 = 0.94$) than for surface coverage ($F(1,16) = 145.90$, $p < 0.001$, $\eta_p^2 = 0.90$). Both models fit the data well, explaining 91.0% and 94.2% of the variation respectively (adjusted R^2).

Residuals were normally distributed for both surface coverage (Shapiro–Wilk $p = 0.213$) and particle count (Shapiro–Wilk $p = 0.060$). Homogeneity of variance was satisfied for both models (Levene $p = 0.468$ and $p = 0.780$ respectively).

The effect of charging depended on the material for both metrics (coverage: $F(3,16) = 5.75$, $p = 0.007$, $\eta_p^2 = 0.52$; count: $F(3,16) = 16.50$, $p < 0.001$, $\eta_p^2 = 0.76$).

Source of variation	df	F	p	η_p^2
(a) Surface coverage				
Material	3	25.84	2.3×10^{-6}	0.83
Voltage	1	145.90	1.9×10^{-9}	0.90
Material × voltage	3	5.75	7.2×10^{-3}	0.52
Residual	16			

(b) Particle count				
Material	3	30.63	7.3×10^{-7}	0.85
Voltage	1	242.09	4.4×10^{-11}	0.94
Material × voltage	3	16.50	3.8×10^{-5}	0.76
Residual	16			

Table 2. Two-way ANOVA for the effects of material and voltage on log10-transformed (a) surface coverage and (b) particle count. Effect sizes are reported as partial eta squared (η_p^2).

4.4 Differences between materials

Table 3 summarizes the improvement factors associated with applying voltage for both metrics. Copper improved the most on both metrics with a 114-fold increase in surface coverage (95% CI: 21–605) and 53.6-fold in particle count (95% CI: 6.9–415). Brass and stainless steel improved by similar amounts and cannot be separated by the data: coverage increased 18.2-fold for brass (95% CI: 1.5–215) and 25.7-fold for stainless steel (95% CI: 3.3–200), while count increased 26.6-fold (95% CI: 8.2–86) and 22.3-fold (95% CI: 15.0–33.1) respectively. With three trials for each condition, the CIs are large. However, all six CIs were greater than one, suggesting that charging improved capture for each of the three materials on both metrics. For aluminum, coverage increased 5.48-fold (95% CI: 3.4–8.9; p = 0.001) but count only increased 1.96-fold (95% CI: 0.61–6.33; p = 0.149). Its coverage CI does not include 1 but its count CI includes 1, making its count improvement not significant (Figure 5).

Material	**Coverage improvement (95% CI)**	**p**	**Count improvement (95% CI)**	**p**
Aluminum	5.48 (3.4 to 8.9)	0.001	1.96 (0.61 to 6.33)	0.149
Brass	18.2 (1.5 to 215)	0.034	26.6 (8.2 to 86)	0.006
Copper	114 (21 to 605)	0.005	53.6 (6.9 to 415)	0.012
Stainless steel	25.7 (3.3 to 200)	0.020	22.3 (15.0 to 33.1)	<0.001

Table 3. Improvement factors for surface coverage and particle count calculated as the ratio of the charged geometric mean to the uncharged geometric mean. Values are reported with 95% CIs and corresponding p-values.

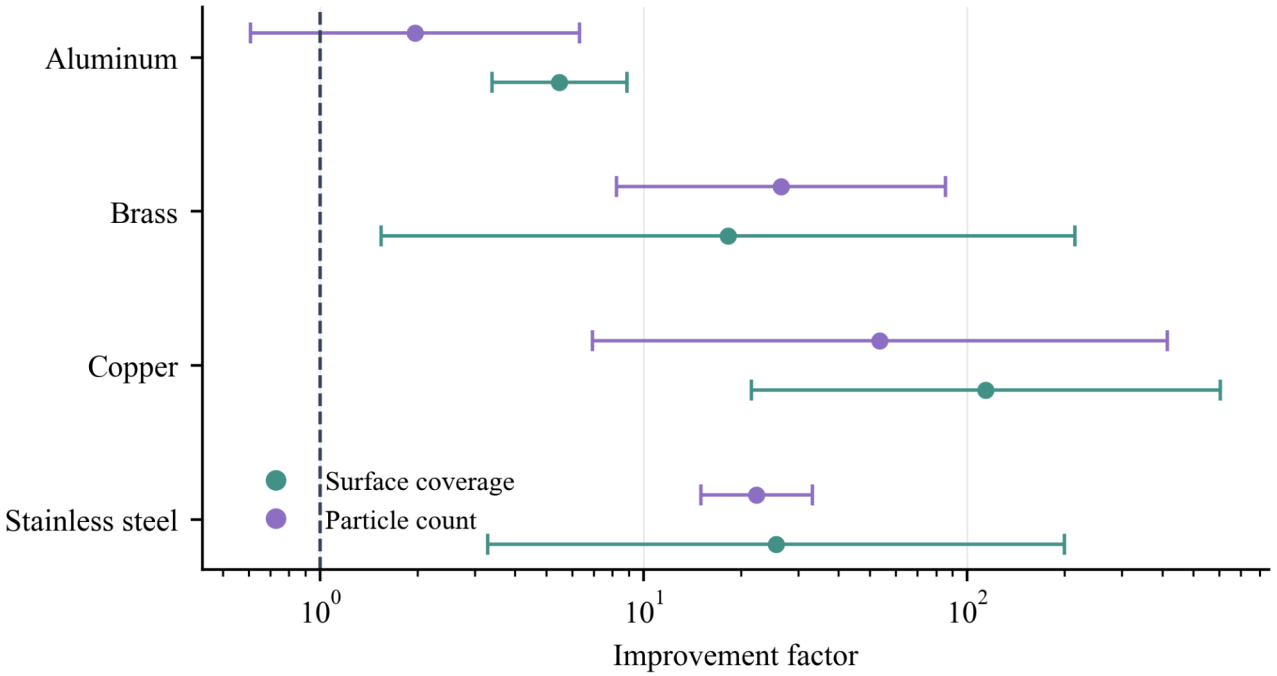

Figure 5. Improvement factors for coverage and particle count with 95% CIs. The dashed line represents no difference between uncharged and charged conditions.

Tukey's HSD test was performed for both metrics in the charged state (Table 4). Copper and brass performed similarly on both metrics (surface coverage: 1.40-fold difference, p = 0.872; particle count: 1.67-fold difference, p = 0.268), and both captured more TWPs than aluminum and stainless steel across both metrics.

Surface coverage was similar between aluminum and stainless steel (2.25-fold difference, p = 0.334), whereas stainless steel captured significantly more particles than aluminum (2.74-fold difference, p = 0.019). The particle count model demonstrates stronger agreement with the data than the coverage model (Section 4.3), suggesting the particle count comparison is more reliable of the two. Both metrics improve for all materials, and in both cases, aluminum has the smallest improvement (Figure 6).

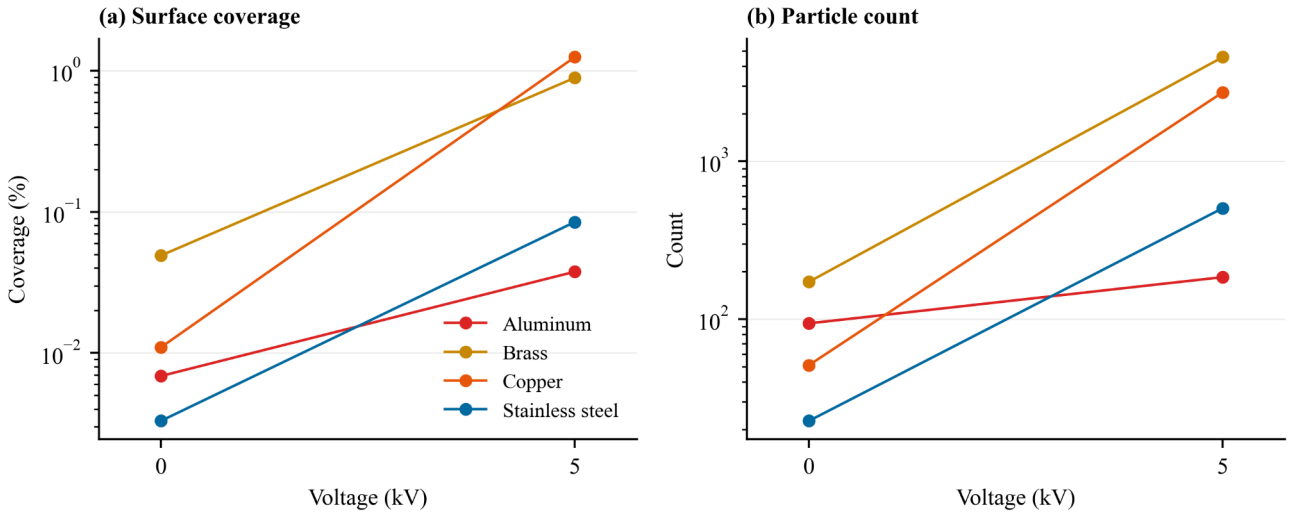

Figure 6. Interaction between plate material and voltage for surface coverage (a) and particle count (b).

Comparison	Coverage, fold difference	p	Count, fold difference	p
Aluminum vs brass	23.7	0.001	24.8	<0.001
Aluminum vs copper	33.2	<0.001	14.8	<0.001
Aluminum vs stainless steel	2.25	0.334	2.74	0.019
Brass vs copper	1.40	0.872	1.67	0.268
Brass vs stainless steel	10.5	0.003	9.06	<0.001
Copper vs stainless steel	14.8	0.001	5.42	<0.001

Table 4. Tukey's HSD comparisons between the four materials in the charged state. Fold difference is the ratio of the two materials' charged geometric means, calculated as the larger value divided by the smaller value.

4.5 Robustness of the material × voltage interaction

A sensitivity analysis was performed to determine if the material × voltage interaction depended disproportionately on a single material. Since aluminum was the only material whose two metrics differed, the two-way ANOVA was repeated without aluminum.

Excluding aluminum strengthened the effect of voltage on both metrics (coverage: $F(1,12) = 111.87$; count: $F(1,12) = 270.26$) and left the effect of material significant (coverage: $F(2,12) = 19.85$; count: $F(2,12) = 34.18$), all $p < 0.001$. The material × voltage interaction was no longer significant for either metric (coverage: $F(2,12) = 2.70$, $p = 0.108$; count: $F(2,12) = 1.63$, $p = 0.237$).

The sample size also decreases without aluminum, though this cannot solely explain why the interaction was not significant. η_p^2 for the interaction decreased from 0.52 to 0.31 for surface coverage and from 0.76 to 0.21 for particle count, suggesting that aluminum explains both interactions. Among brass, copper, and stainless steel, charging produced similar proportional improvements, suggesting that their performance differences were due to a difference in uncharged collection ability, not their responses to electrostatic charging.

5. Discussion

5.1 Findings

The magnitude of TWP capture depends on the material used. Brass, copper, and stainless steel improved significantly on both metrics, with copper gaining the most at 114 times the coverage and 53.6 times the particle count. Aluminum improved significantly on coverage (5.5-fold) but not particle count. When charged, copper and brass captured significantly more than either aluminum or stainless steel on both measures.

The ranking in performance aligns inversely with the band gaps of the oxide layer on each plate. Copper's film consists of Cu_2O and CuO with band gaps of 2.2 eV and 1.2 eV respectively [18]. Brass has a mixed copper and zinc oxide layer, with ZnO at 3.3 eV [19]. Stainless steel has a Cr_2O_3 layer at 3.6-3.7 eV [20] and aluminum has an amorphous Al_2O_3 film at 7.0 ± 0.1 eV [21]. The surface coverage of the materials when charged aligns inversely with these values, with copper (1.250%), brass (0.892%), stainless steel (0.085%), and

then aluminum (0.038%). Even though ZnO and Cr_2O_3 differ minimally, brass and stainless steel differ tenfold in coverage when charged ($p = 0.003$); brass was also more similar to copper than stainless steel for both metrics. Thus, the copper oxide may have had a larger influence on the surface properties of brass than ZnO. Nevertheless, the composition and thickness of the oxide films of the plates were not measured so their surface chemistry is only a hypothesis.

5.2 Charge polarity of captured particles

The observation that particles were only seen on the negatively charged plate suggests that the TWPs carried positive charges. The patent by The Tyre Collective [8] indicates that carbon in tire particles become positively charged. It also notes that insulating constituents charge positively under friction and conducting constituents charge negatively. The inference that particles were positively charged suggests that the tire was made of insulating material. The balance of particle polarity is difficult to predict because tire tread is a heterogeneous composite and abrasion can influence the charge transfer.

This finding can influence collector designs. For example, a collector can hold every other plate at a negative potential and ground the other plates instead of alternating positive and negative. Still, these designs must be tested and TWP distribution between positively and negatively charged plates must be explored further.

5.3 Evaluation

The proposed method has several limitations. A bicycle tire spun against sandpaper does not fully reproduce tire-road contact, so the particles are not TRWPs. Laboratory-generated particles can substantially differ from road-collected particles in size and composition [22,23], which is also influenced by real-world airflow and humidity. The generated particles were not chemically measured, so there is potential for contributions from the sandpaper. Electron microscopy would confirm the composition. In addition, the number of trials in the experiment is small ($n = 3$), resulting in wide CIs. At the image resolution used, one pixel corresponds to approximately 110 μm. Particles below this threshold were not isolated, so the reported mean diameters (340–860 μm) reflect the coarse TWPs on the plate. However, this does not affect comparisons between materials.

An extension is to measure TWP capture across a range of voltages. Measuring the surface properties of each metal would test the oxide-conductivity discussed in Section 5.1, which the present data only supports indirectly. Testing under controlled humidity and airflow conditions is a potential improvement to the relevance of the results.

6. Conclusion

A methodology for measuring the effect of material on electrostatic capture of TWPs was proposed. At 5 kV, copper and brass captured about twenty times more material than aluminum or stainless steel. Charging improved capture for brass, copper, and stainless steel on both metrics, most strongly for copper (114-fold in surface coverage, 53.6-fold in particle count). Aluminum improved significantly on surface coverage but not on particle count. Visible captured particles occurred only on the negatively charged plate of each pair. These findings need to be confirmed with a wider voltage range and improved image acquisition techniques.

Funding declaration

This research did not receive any specific grant from funding agencies in the public, commercial, or not-for-profit sectors.

Data availability

All data generated in the study are provided in Table A1. Plate images and thresholded images will be made available on request.

References

[1] A. Piscitello, C. Bianco, A. Casasso, and R. Sethi, "Non-Exhaust Traffic Emissions: Sources, Characterization, and Mitigation Measures," *Science of The Total Environment*, vol. 766, p. 144440, Apr. 2021, doi: 10.1016/j.scitotenv.2020.144440.

[2] B. Giechaskiel *et al.*, "Contribution of Road Vehicle Tyre Wear to Microplastics and Ambient Air Pollution," *Sustainability*, vol. 16, no. 2, p. 522, Jan. 2024, doi: 10.3390/su16020522.

[3] B. Baensch-Baltruschat, B. Kocher, F. Stock, and G. Reifferscheid, "Tyre and Road Wear Particles (TRWP) - a Review of Generation, Properties, Emissions, Human Health Risk, Ecotoxicity, and Fate in the Environment," *Science of The Total Environment*, vol. 733, p. 137823, Sep. 2020, doi: 10.1016/j.scitotenv.2020.137823.

[4] Z. Tian *et al.*, "A Ubiquitous Tire Rubber–Derived Chemical Induces Acute Mortality in Coho Salmon," *Science*, vol. 371, no. 6525, pp. 185–189, Jan. 2021, doi: 10.1126/science.abd6951.

[5] Y. Jiang *et al.*, "Human Airway Organoids as 3D in Vitro Models for a Toxicity Assessment of Emerging Inhaled Pollutants: Tire Wear Particles," *Frontiers in Bioengineering and Biotechnology*, vol. 10, p. 1105710, Jan. 2023, doi: 10.3389/fbioe.2022.1105710.

[6] A. Bouredji, J. Pourchez, and V. Forest, "Biological Effects of Tire and Road Wear Particles (TRWP) Assessed by in Vitro and in Vivo Studies – a Systematic Review," *Science of The Total Environment*, vol. 894, p. 164989, Oct. 2023, doi: 10.1016/j.scitotenv.2023.164989.

[7] Y. Xu *et al.*, "Fresh Tire Wear Particles From Moving Vehicles: Dispersion Dynamics, Exposure, and Prevention Strategy," *Emerging Contaminants*, vol. 11, no. 3, p. 100503, Sep. 2025, doi: 10.1016/j.emcon.2025.100503.

[8] C. P. H. Cheng, H. Richardson, S. L. Anderson, and M. D. Mallya, "Particulate Collecting Device," Aug. 05, 2021 Accessed: Jul. 30, 2026. [Online]. Available: https://patents.google.com/patent/WO2021152331A1/

[9] S.-H. Woo *et al.*, "An Active-Type Dust Collector That Reduces Brake Wear Particle (BWP) Emission," *Aerosol Science and Technology*, vol. 58, no. 11, pp. 1293–1304, Aug. 2024, doi: 10.1080/02786826.2024.2385642.

[10] S.-H. Woo *et al.*, “Development of a Brake Wear Particle Collector Utilizing a Forced-Floating Concept for Euro-7 Compliance,” *Aerosol Science and Technology*, vol. 60, no. 3, pp. 197–212, Dec. 2025, doi: 10.1080/02786826.2025.2601179.

[11] Y. Lee *et al.*, “Removal of Mist Particles by a Two-Stage Electrostatic Precipitator Featuring Plastic Plate Electrodes,” *IEEE Transactions on Industry Applications*, vol. 58, no. 3, pp. 3985–3991, Mar. 2022, doi: 10.1109/tia.2022.3159306.

[12] J.-Y. Syu *et al.*, “The Applications and Distinctions of Three Different Material Collection Plates in Wet Electrostatic Precipitator,” *Aerosol and Air Quality Research*, vol. 22, no. 10, p. 220133, 2022, doi: 10.4209/aaqr.220133.

[13] S. Ratanaporn, W. Bunriw, V. Harnchana, and K. Banlusan, “Electrostatic Energy-Driven Contact Electrification Mechanism From the ReaxFF Molecular Dynamics Perspective,” *J. Chem. Phys.*, vol. 161, no. 9, p. 094702, Sep. 2024, doi: https://doi.org/10.1063/5.0217824.

[14] O. Verners *et al.*, “Smooth Polymers Charge Negatively: Controlling Contact Electrification Polarity in Polymers,” *Nano Energy*, vol. 104, p. 107914, Dec. 2022, doi: 10.1016/j.nanoen.2022.107914.

[15] W. Deutsch, “Bewegung Und Ladung Der Elektrizitätsträger Im Zylinderkondensator,” *Annalen der Physik*, vol. 373, no. 12, pp. 335–344, Jan. 1922, doi: 10.1002/andp.19223731203.

[16] A. G. Bailey, “Electrostatic Phenomena During Powder Handling,” *Powder Technology*, vol. 37, no. 1, pp. 71–85, Jan. 1984, doi: 10.1016/0032-5910(84)80007-8.

[17] C. A. Schneider, W. S. Rasband, and K. W. Eliceiri, “NIH Image to ImageJ: 25 Years of Image Analysis,” *Nature Methods*, vol. 9, no. 7, pp. 671–675, Jun. 2012, doi: 10.1038/nmeth.2089.

[18] Y. Wang *et al.*, “Electronic structures of Cu_2O, Cu_4O_3, and CuO: A joint experimental and theoretical study,” *Physical review*, vol. 94, no. 24, Dec. 2016, doi: 10.1103/physrevb.94.245418.

[19] V. Srikant and D. R. Clarke, “On the Optical Band Gap of Zinc Oxide,” *Journal of Applied Physics*, vol. 83, no. 10, pp. 5447–5451, May 1998, Accessed: Aug. 03, 2026. [Online]. Available: https://doi.org/10.1063/1.367375

[20] H. Tsuchiya, S. Fujimoto, O. Chihara, and T. Shibata, “Semiconductive Behavior of Passive Films Formed on Pure Cr and Fe–Cr Alloys in Sulfuric Acid Solution,” *Electrochimica Acta*, vol. 47, no. 27, pp. 4357–4366, Oct. 2002, doi: 10.1016/s0013-4686(02)00508-x.

[21] E. O. Filatova and A. S. Konashuk, “Interpretation of the Changing the Band Gap of Al2O3 Depending on Its Crystalline Form: Connection With Different Local Symmetries,” *The Journal of Physical Chemistry C*, vol. 119, no. 35, pp. 20755–20761, Aug. 2015, doi: 10.1021/acs.jpcc.5b06843.

[22] M. L. Kreider, J. M. Panko, B. L. McAtee, L. I. Sweet, and B. L. Finley, "Physical and Chemical Characterization of Tire-Related Particles: Comparison of Particles Generated Using Different Methodologies," *Science of The Total Environment*, vol. 408, no. 3, pp. 652–659, Jan. 2010, doi: 10.1016/j.scitotenv.2009.10.016.

[23] R. Stoček, M. Stěnička, M. Pöschl, S. Datta, T. Kramer, and F. Schmerwitz, "Challenges in Tire Wear Particle Collection: A Laboratory Perspective Using DIN Abrasion Testing," *Wear*, vol. 601, p. 206843, Sep. 2026, doi: 10.1016/j.wear.2026.206843.

Appendix A

Material	Trial	Voltage	Particle count	Total particle area (mm^2)	Coverage (%)
Aluminum	1	0 kV	113	10.7	0.009
Aluminum	2	0 kV	94	8.4	0.006
Aluminum	3	0 kV	78	7.5	0.006
Aluminum	4	5 kV	215	45.7	0.033
Aluminum	5	5 kV	102	44.7	0.045
Aluminum	6	5 kV	286	33.2	0.036
Brass	1	0 kV	96	14.8	0.013
Brass	2	0 kV	229	74.7	0.070
Brass	3	0 kV	232	142.4	0.130
Brass	4	5 kV	3971	267.0	0.452
Brass	5	5 kV	4967	1166.1	1.461
Brass	6	5 kV	4843	648.1	1.075
Copper	1	0 kV	18	4.9	0.005
Copper	2	0 kV	90	22.4	0.022
Copper	3	0 kV	82	14.6	0.012
Copper	4	5 kV	3091	2294.0	1.448
Copper	5	5 kV	3264	1563.9	1.408
Copper	6	5 kV	2030	1045.0	0.959
Stainless steel	1	0 kV	21	3.7	0.004
Stainless steel	2	0 kV	23	2.6	0.003
Stainless steel	3	0 kV	24	3.0	0.003
Stainless steel	4	5 kV	412	85.4	0.102
Stainless steel	5	5 kV	531	137.2	0.181
Stainless steel	6	5 kV	587	37.9	0.033

Table A.1. Raw data from ImageJ for all 24 trials.